

***s*-wave pairing in MgCNi₃ revealed by point contact tunneling**

L. Shan, H. J. Tao, H. Gao, Z. Z. Li, Z. A. Ren, G. C. Che, and H. H. Wen*

National Laboratory for Superconductivity, Institute of Physics, Chinese Academy of Sciences, P.O. Box 603, Beijing 100080, China

(Received 13 June 2003; revised manuscript received 24 July 2003; published 7 October 2003)

Electron-tunneling spectroscopy on MgCNi₃ has been studied with N/MgCNi_3 point contacts with $N = \text{PtIr}$ and Au. Most of the measured tunneling conductance show an Andreev reflection peak and a pronounced dip structure outside the peak. We introduce a Josephson junction in series with the point contact to model the tunneling process. By tuning the weights of the point contact quasiparticle voltage and the Josephson voltage we are able to fit almost all the tunneling data nicely. The results support BCS *s*-wave pairing in MgCNi₃, and the model explains the sharp dip structure which is seen in point contact tunneling into some polycrystalline superconductors.

DOI: 10.1103/PhysRevB.68.144510

PACS number(s): 74.50.+r, 74.20.Rp, 74.70.Dd

The discovery of superconductivity in MgCNi₃ (Ref. 1) seems to be surprising due to the strong ferromagnetic instability in this system.² It is argued that the nonoxide perovskite superconductor could be a bridge between conventional superconductors and high- T_c cuprates. So the issue on whether it is a conventional or an unconventional superconductor has attracted considerable interest. On the experimental side, the NMR experiment exhibited a clear coherence peak of the nuclear spin-lattice relaxation rate just below T_c ,³ suggesting conventional pairing. Specific-heat measurement also showed conventional BCS-like superconductivity in MgCNi₃,⁴ while recent low-temperature London penetration depth measurement reported by Prozorov *et al.*⁵ exhibited distinctly non-*s*-wave behavior, indicating a possibly nodal order parameter in MgCNi₃. Controversial reports also resulted from tunneling measurements: low-temperature scanning tunneling spectroscopy study supported BCS *s*-wave weak-coupling superconductivity in MgCNi₃,⁶ while the point contact tunneling measurements done by Mao *et al.*⁷ suggested the possibility of non-*s*-wave strong-coupling superconductivity based on the observation of sharp zero-bias conductance peaks (ZBCP). Theoretically, a unique multiband *s*-wave picture has been predicted to reconcile apparently contradictory experimental observations.⁸ By considering a possible magnetic coupling strength due to spin fluctuations,⁹ Shan *et al.* have proposed¹⁰ that the superconductivity in this system originates from the conventional electron-phonon coupling while it is depressed by the electron-magnon coupling.

To explore the pairing symmetry in MgCNi₃ and to determine the superconducting gap value, point contact tunneling spectroscopy has been investigated with high quality polycrystalline MgCNi₃ samples using PtIr and Au tips. The measured tunneling conductance are dominantly of classic Andreev reflection type, but with an additional dip structure outside the central peak, which cannot be accounted for by the Blonder-Tinkham-Klapwijk (BTK) theory.¹¹ We introduce a Josephson junction in series with a normal-metal/superconductor (N/S) point contact to model the tunneling. By tuning the weights of the point contact Andreev reflection voltage and the Josephson voltage we are able to fit the ob-

tained tunneling data remarkably well. The results are consistent with BCS *s*-wave pairing in MgCNi₃, and the model explains similar sharp dip feature appeared in data from point contact tunneling into polycrystalline superconductor MgB₂.¹²

The polycrystalline MgCNi₃ used in this study was prepared by powder metallurgy method. Details of the preparation can be found in Ref. 13. X-ray-diffraction pattern showed that the sample was nearly of single phase, and ac susceptibility measurement indicated that the superconducting transition temperature T_c was 7 K with a transition width of 0.5 K.¹⁰ The samples were cut into wafers with radius of 3 mm and thickness of 0.5–1 mm. Their surfaces were polished by fine metallographic grinding papers and then milled by Ar iron for 20–30 min. Then the samples were cleaned with pure ethanol in an ultrasonic bath for 5 min, followed by being blown dried just before being mounted onto the point contact insert. The PtIr tips were prepared by electrochemical etching in CaCl₂ solution with Pt_{0.9}Ir_{0.1} wire with a diameter of 0.25 mm. The Au tips were fabricated mechanically by finely grinding a gold wire with a diameter of 1 mm. Finally, the tips were cleaned with distilled water to eliminate residuum. The approaching of the tips was controlled by a differential screw. The point contact insert was set in the sample chamber of an Oxford cryogenic system Maglab. Typical four-terminal and lock-in techniques were used to measure the differential resistance dV/dI vs V of the point contacts. Then the dV/dI - V curves were converted into the dynamical conductance dI/dV - V (or σ - V) curves, and the normalized conductance curves (σ/σ_N - V) were obtained by dividing dI/dV - V with one of its high-bias value (σ_N).

In Fig. 1 we present, by open circles, four typical normalized conductance (σ/σ_N) of PtIr/MgCNi₃ point contacts measured at 1.7 K. The common features for these four figures are the following. A central Andreev-reflection-like peak and two sharp dip structures appeared symmetrically on each side of it; the only difference between them is the detailed shape of the Andreev-reflection-like peak: with a zero bias dip [Fig. 1(a) and 1(b)], a sharper peak [Fig. 1(c)], and a nearly flat top with a magnitude higher than 2 [Fig. 1(d)]. Disregarding the dip structure, all these curves except for the last one can be well fitted with the generalized BTK theory¹¹ with BCS density of states (DOS), in which the quasiparticle

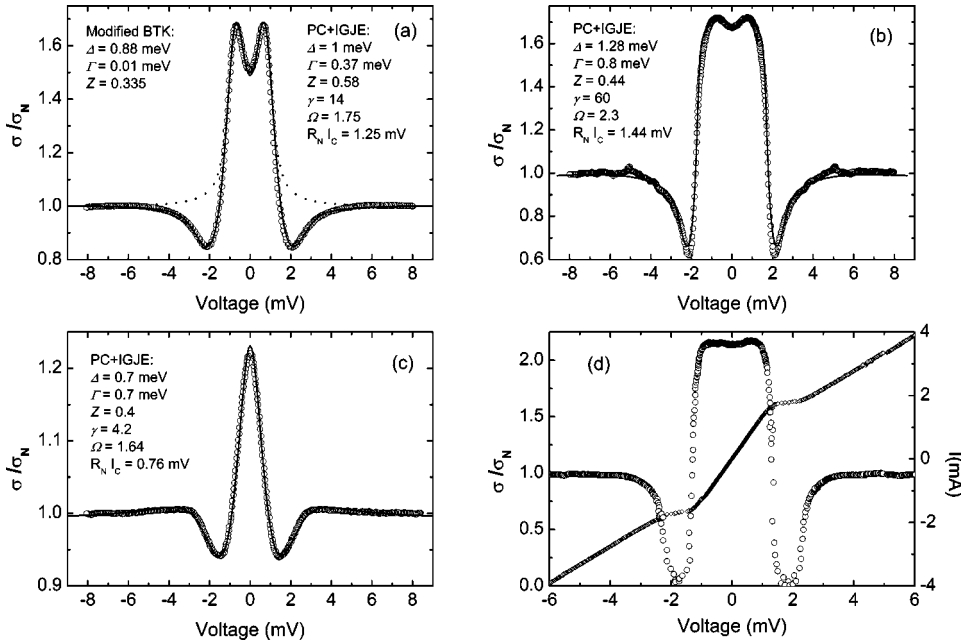


FIG. 1. Some typical experimental normalized conductance curves (open circles) of our PtIr/MgCNi₃ point contacts measured at 1.7 K. (a), (b) and (d) are obtained from the Ar-ions milled surface, while (c) corresponds to the unmilled surface. The dotted line in (a) is the fit to the modified BTK theory. The solid lines represent the fits to the model proposed in Eq. (2).

energy E is replaced by $E + i\Gamma$, where Γ is the smearing parameter characterizing the finite lifetime of the quasiparticles.¹⁴ According to this theory, the height and splitting of Andreev reflection peak are dominated by the barrier Z , its width is dominated by the energy gap Δ , but all these characteristics will be smeared by temperature and the introduction of Γ . An example of the BTK fit is given in Fig. 1(a) by the dotted line. However, before we can conclude that the order parameter in the MgCNi₃ is of BCS s -wave symmetry, two questions should be answered: (a) What is the origin of the dip structure in these tunneling spectra and (b) How to reconcile the magnitude of the central Andreev-reflection-like peak which in some cases is greater than 2 [as shown in Fig. 1(d)]. Large ZBC peak, greater than 2, was the key feature observed by Mao *et al.*,⁷ and based on it they predicted the non- s -wave superconducting gap in the MgCNi₃. We will show that the two abnormal features in fact stem from the same origin.

To show the high quality of the point contacts and to further illustrate the Andreev reflection characteristic of the obtained tunneling conductance, we present, as an example, in Fig. 2 the conductance at different temperatures (T) using one PtIr/MgCNi₃ point contact. The curves of different T are shifted vertically for clarity. As can be seen both the central peak and the dip structure are depressed with increase of T , and disappear at T_c , indicating both structures to be related to superconduction. Apart from the dip structure, there is no doubt that the conductance are of the classic Andreev reflection type. Moreover, these features are reproducible in several successive measurements, implying a quite stable physical mechanism. Then what is the origin of the repeatedly appeared dip structure? First, it is not likely caused by strong-coupling effect,^{15,16} due to the remarkable difference of its shape and energy location between various spectra measured at different points on the sample surface. Second, it is also different from that caused by proximity effect.¹⁷ For very thin normal layer residing in between the tip and the

MgCNi₃ sample, the dip structure is interpreted as the de Gennes bound state, and the position of the minimum of the dip gives the measurement of the superconducting gap (Δ) of the bulk superconductor.¹⁸ If we take the dip's position as the gap, the determined (Δ) of MgCNi₃ can be as large as 2.5 meV, which is much larger than the result of specific-heat measurement⁴ and leads to an unreasonable strong-coupling parameter $2\Delta/k_B T_c > 8.3$. Meanwhile, it is also unreasonable to assume that the dip structure originates from proximity effect by very thick normal layer as those predicted by McMillan and Tomasch, because the dips look sharp and deep, and no oscillation has been observed.

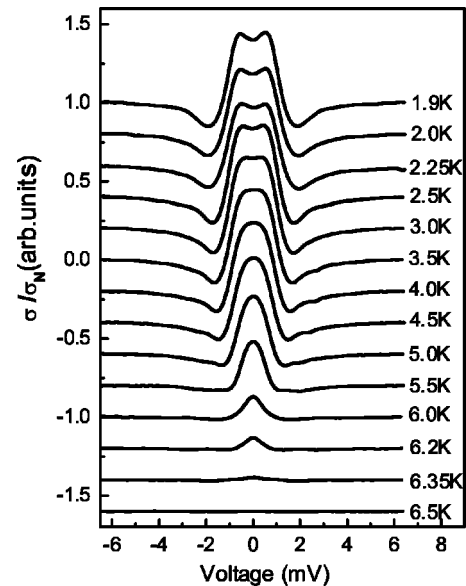


FIG. 2. Temperature dependence of the Andreev reflection spectra for PtIr/MgCNi₃ point contact at a fixed point on the sample surface. All curves except the top curve have been shifted downwards for clarity.

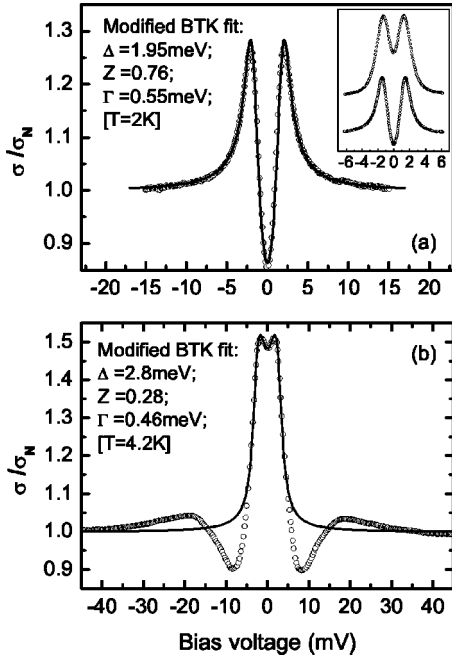


FIG. 3. The typical Andreev reflection spectra of PtIr/Nb point contact measured at 2 K (a) and that of PtIr/MgB₂ point contact measured at 4.2 K (Ref. 12) (b). The experimental data are denoted by open circles. The solid lines represent the fits to the modified BTK theory.

In order to find out the origin of the dip structure, we have comparatively investigated the tunneling spectroscopy of PtIr/Nb-foil and PtIr/MgB₂-polycrystal point contacts. In Fig. 3(a) and 3(b) we show the typical tunneling spectra of the PtIr/Nb and PtIr/MgB₂ point contacts taken at 2 K and 4.2 K, respectively. The qualitative difference between these two kinds of spectra is apparent. No dip structure can be found in the tunneling spectra of the PtIr/Nb-foil point contacts, and the curves can be well fitted to the BTK theory. On the contrary, the dynamic conductance of the PtIr/MgB₂-polycrystal point contact shown in Fig. 3(b) displays clear dip structure, apart from the typical Andreev reflection peak which is very similar to those shown in Fig. 1. The comparative study gave a clue to link the dip structure to the polycrystalline nature of the MgB₂ sample. In fact the dip structure is seen in point contact tunneling of N/MgB₂ polycrystal.^{12,19–22}

We speculate that the intergrain weak-coupling effect of the polycrystalline samples plays a role in the tunneling process for the metal/MgB₂ and N/MgCNi₃ point-contact junctions, namely, there is a S/I/S or S/N/S Josephson junction that is connected with the point contact in series. A familiar appearance of such effect is a ZBC peak in the high barrier tunneling spectra,^{19,23} which has been ascribed to the existence of Josephson effect due to the loosely connected single grains. And the appearance of the Josephson voltage, large or small, is responsible for the observed dip structure in the tunneling conductance. The point contact has been intentionally used as a method to realize S/I/S break junction for the studies of tunneling spectroscopy of the high-T_c supercon-

ductor Bi2212,^{16,24,25} where the effect of point contact is almost completely covered up by the Josephson junction.

According to above discussions, the intergrain Josephson effect (IGJE) has to be taken into account in order to quantitatively describe the measured tunneling spectra. Considering a real junction between a metal tip and a polycrystalline sample, point contact is formed by the tip apex and a single grain which contacts the bulk sample with an intergrain Josephson junction. That is, in our experiments, the measured voltage includes two contributions coming from the series-connected point contact and Josephson junction, respectively. Under the condition that a small capacitance *C* and the thermal noise are present, the contribution of IGJE can be simulated by the modified resistively shunted junction (RSJ) model given by Lee:²⁶

$$\langle V_{IGJE} \rangle = \frac{2}{\gamma} R_N I_c \frac{\exp(\pi \gamma \alpha) - 1}{\exp(\pi \gamma \alpha)} T_1^{-1} \left(1 + \Omega^2 \frac{T_2}{T_1} \right), \quad (1a)$$

$$T_1 = \int_0^{2\pi} d\varphi I_0 \left(\gamma \sin \frac{\varphi}{2} \right) \exp \left[- \left(\frac{\gamma}{2} \right) \varphi \right], \quad (1b)$$

$$T_2 = \int_0^{2\pi} d\varphi \sin \frac{\varphi}{2} I_1 \left(\gamma \sin \frac{\varphi}{2} \right) \exp \left[- \left(\frac{\gamma}{2} \right) \varphi \right], \quad (1c)$$

where $\langle V_{RSJ} \rangle$ is the average voltage corresponding to the measurable dc value, *I_c* is the maximum Josephson current, *R_N* is the normal-state resistance, $\alpha = I/I_c$ is the normalized current, $\gamma = hI_c / (ek_B T_n)$ in which *T_n* is the effective noise temperature, $\Omega = (2eI_c C / \hbar)^{1/2} R_N$, and *I₀*(*x*) and *I₁*(*x*) are the modified Bessel functions. Meanwhile, the voltage contribution of point contact (*V_{PC}*) can be simulated by the modified BTK theory. Thus we can calculate the current-voltage (I-V) characteristic or the differential conductance $\sigma(V)$ by using the following relations:

$$V(I) = V_{PC}(I) + V_{IGJE}(I), \quad (2a)$$

$$\sigma(V) = dI/dV = (dV_{PC}/dI + dV_{IGJE}/dI)^{-1}. \quad (2b)$$

It should be emphasized that not all the measured curves can be fitted in terms of this model which is in the limit of small capacitance. In order to elucidate this issue and visualize our model, we show our fitting process in Fig. 4, the raw data are the same as that in Fig. 1(b). It can be seen in Fig. 4 that the total voltage includes two parts as discussed above. When the current is lower than the critical current of IGJE, $V_{IGJE} \approx 0$ and hence *V_{PC}* is the main contribution to the total voltage, therefore the characteristics of the point contact dominate the low bias spectrum. However, with the increase of bias voltage, a remarkable enhancement of *V_{IGJE}* will occur when the current is around the critical current of IGJE, which produces a dip in the spectrum [or $\sigma(V)$ curve]. Above this region, the spectrum is dominated by either *V_{PC}* or *V_{IGJE}* according to the magnitude of their normal-state resistance. From Fig. 4, we can estimate the normal-state resistance of point contact and IGJE as *R_{PC}* = 0.6 Ω and *R_{IGJE}* = 0.26 Ω, respectively. Therefore, in this case, both the point contact and IGJE are crucial to the measured spectral shape. According to the above discussion, the fitting pat-

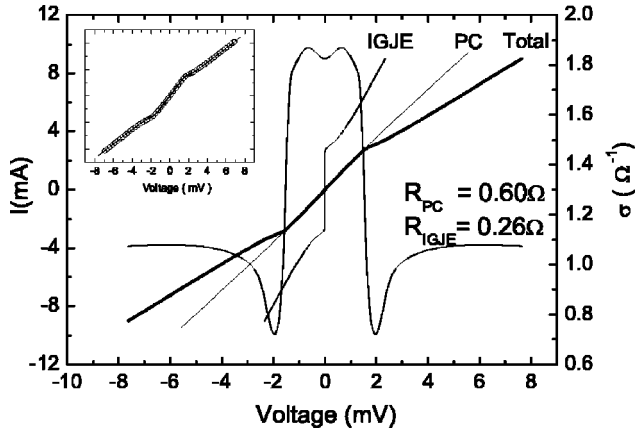


FIG. 4. Detailed process of fitting the data shown in Fig. 1(b). Inset: the original I - V curve (open circles) and theoretical simulation (solid line).

rameters of the modified BTK theory and the modified RSJ model are dominated by the central Andreev reflection peak and the dip structure, respectively. Moreover, the modified RSJ model is based on the case of small capacitance, in which the voltage change is mild around the critical current and hence the dips in the spectra are not very deep. However, for the case of large capacitance, the voltage change is very sharp at the critical current and hence the dips are very deep even to zero as shown in Fig. 1(d). In this case, the modified RSJ model is not appropriate and there is no analytical expression to describe the measured curves; we will try to clarify this problem by numerical calculation elsewhere.

The typical fits to the differential conductance with Eq. (2) are presented in Fig. 1 by solid lines. The determined values of superconducting gap Δ vary from 0.7 meV to 1.3 meV, depending on the quality of various sample surfaces or different points on the same surface. The larger gaps $\Delta > 1$ meV are readily obtained from the Ar-ions milled surfaces, while for the unmilled surfaces, most of the Δ values are smaller than 1 meV. Therefore, considering the degradation of the sample surface, the gap determined here should be smaller than the bulk superconducting gap. Nonetheless, by taking the maximum gap of 1.3 meV as the bulk gap, we obtain the coupling parameter $2\Delta/k_B T_c = 4.3$, which is in good agreement with the results of specific-heat measurements reported by Lin *et al.*⁴ and Mao *et al.*⁷ ($2\Delta/k_B T_c = 4.0$ and 4.4 , respectively).

Up to now, we have ascribed the dip structure observed in Andreev reflection spectra to the IGJE. In order to get more convincing evidence for this explanation, we have remeasured the tunneling spectra on a Au/MgCNi₃ point contact. Because Au is much softer than PtIr alloy, we can get a fine metallic contact between Au tip and the MgCNi₃ grain by tightly pressing the tip to the sample surface. As a consequence, the tip apex is not sharp any longer and the point contact should become a plane contact. Therefore, the spectral characteristics of Andreev reflection effect become much weaker than that of the fine point contact. In this case, the IGJE should dominate the spectrum regardless of the exact spectral shape of the point contact. In Fig. 5, we present the

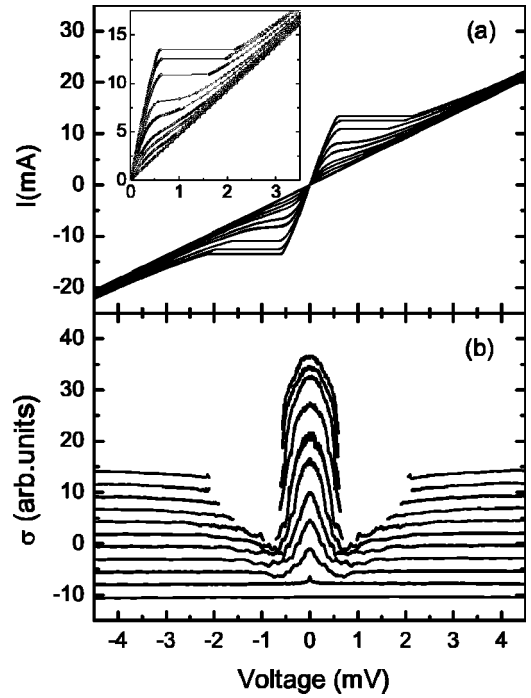


FIG. 5. (a) Current-voltage characteristics of the Au/MgCNi₃ point contact at different temperatures. Inset shows the details at low bias. (b) Temperature dependence of the tunneling conductance calculated from the curves in (a) by differential, all curves except the top curve have been shifted downwards for clarity. The temperatures (K) from top to bottom are 1.9, 2, 3, 4, 5, 5.5, 6, 6.25, 6.5, 6.75, 7, respectively. Note that the disconnection of the spectra in (b) is due to the abrupt voltage jump around critical current as shown in (a).

temperature dependence of the I - V characteristics and the differential conductance of the Au/MgCNi₃ contact, which indeed exhibits the combination of a nearly normal resistance and a typical Josephson junction. Therefore, the following relation should be a reasonable approach:

$$V = IR_{PC} + V_{IGJE}, \quad (3a)$$

$$\sigma(V) = (R_{PC} + dV_{IGJE}/dI)^{-1}. \quad (3b)$$

Here, we should also emphasize that the modified RSJ model cannot describe the V_{IGJE} in Fig. 5 due to the abrupt voltage jump when critical current is achieved. Similar to the foregoing discussions, this should be due to the large capacitance. Fitting such typical Josephson-type curves needs more onerous numerical calculations, we thus leave this issue to a future work. Nonetheless, from these data, it is easily understood that why the ZBCP observed in the normalized conductance σ/σ_N can be higher than 2 (the maximum value expected for the conventional Andreev reflection) as reported in Ref. 7. It is well known that, for a pure Josephson junction, the height of ZBCP can be very high. However, for the case in this work, the resistance of point contact may badly depress the height of ZBCP. Hence, the actual height of ZBCP is determined by not only the property of IGJE but also the magnitude of resistance of point contact. One should be very careful to distinguish s and so other unconventional

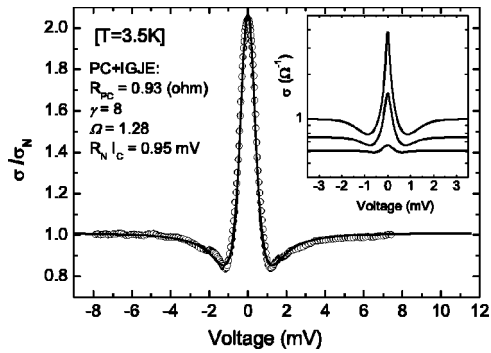


FIG. 6. A random tunneling spectra of Au/MgCNi₃ point contact (open circles). The solid line represents the fit to Eq. (3). Inset: numerical simulations to the temperature-dependent tunneling spectra reported in Ref. 7.

pairing symmetry by tunneling measurement when the IGJE cannot be neglected. In order to quantitatively clarify this problem, we try to fit a typical ZBCP obtained at another point on the sample surface in terms of the above model. As shown in Fig. 6, the good agreement of the experimental data with this simple model indicates the remarkable influence of the IGJE on the tunneling spectra (especially for the Andreev reflection) measurement for those loose polycrystalline

samples. Since the junction resistance reported by Mao *et al.* is quite small ($R_J < 0.1 \Omega$), the IGJE may be a reasonable explanation for the surprising ZBCP presented in their work.⁷ In order to give an intuitive illustration, we quantitatively simulate in the inset of Fig. 6 the temperature dependence of the tunneling spectra presented in Ref. 7.

In summary, we have performed Andreev reflection measurements on the metal/MgCNi₃ point contacts in detail. The clear Andreev reflection spectra can be well fitted in the frame of BTK theory, providing compelling evidence for the conventional s-wave superconductivity in MgCNi₃. A dip structure, which has also been repeatedly observed in the spectra, was proved to be caused by the intergrain Josephson effect. Such a Josephson effect becomes prominent when the point contact resistance is heavily reduced, leading to a high conductance peak at zero bias. This should be responsible for the inconsistency between the previously reported tunneling measurements and other experiments such as NMR and specific-heat measurements.

This work was supported by the National Science Foundation of China, the Ministry of Science and Technology of China (Project No. NKBRSF-G1999064602), and Chinese Academy of Sciences with the Knowledge Innovation Project.

*Electronic address: hhwen@aphy.iphys.ac.cn

- ¹T. He, Q. Huang, A.P. Ramirez, Y. Wang, K.A. Regan, N. Rogado, M.A. Hayward, M.K. Haas, J.S. Slusky, K. Inumara, H.W. Zandbergen, N.P. Ong, and R.J. Cava, *Nature (London)* **411**, 54 (2001).
- ²H. Rosner, R. Weht, M.D. Johannes, W.E. Pickett, and E. Tosatti, *Phys. Rev. Lett.* **88**, 027001 (2002).
- ³P.M. Singer, T. Imai, T. He, M.A. Hayward, and R.J. Cava, *Phys. Rev. Lett.* **87**, 257601 (2001).
- ⁴J.Y. Lin, P.L. Ho, H.L. Huang, P.H. Lin, Y.L. Zhang, R.C. Yu, C.Q. Jin, and H.D. Yang, *Phys. Rev. B* **67**, 052501 (2003).
- ⁵R. Prozorov, A. Snezhko, T. He, and R.J. Cava, *cond-mat/0302431* (unpublished).
- ⁶G. Kinoda, M. Nishiyama, Y. Zhao, M. Murakami, N. Koshizuka, and T. Hasegawa, *Jpn. J. Appl. Phys., Part 2* **40**, L1365 (2001).
- ⁷Z.Q. Mao, M.M. Rosario, K.D. Nelson, K. Wu, I.G. Deac, P. Schiffer, Y. Liu, T. He, K.A. Regan, and R.J. Cava, *Phys. Rev. B* **67**, 094502 (2003).
- ⁸K. Voelker and M. Sigrist, *cond-mat/0208367* (unpublished).
- ⁹D.J. Singh and I.I. Mazin, *Phys. Rev. B* **64**, 140507 (2001).
- ¹⁰L. Shan, K. Xia, Z.Y. Liu, H.H. Wen, Z.A. Ren, G.C. Che, and Z.X. Zhao, *Phys. Rev. B* **68**, 024523 (2003).
- ¹¹G.E. Blonder, M. Tinkham, and T.M. Klapwijk, *Phys. Rev. B* **25**, 4515 (1982).
- ¹²Z.Z. Li, H.J. Tao, Y. Xuan, Z.A. Ren, G.C. Che, and B.R. Zhao, *Phys. Rev. B* **66**, 064513 (2002).
- ¹³Z.A. Ren, G.C. Che, S.L. Jia, H. Chen, Y.M. Ni, G.D. Liu, and Z.X. Zhao, *Physica C* **371**, 1 (2002).
- ¹⁴A. Pleceník, M. Grajcar, S. Benacka, P. Seidel, and A. Pfuch, *Phys. Rev. B* **49**, 10 016 (1994).
- ¹⁵M. Jourdan, M. Huth, and H. Adrian, *Nature (London)* **398**, 47 (1999).
- ¹⁶Y. DeWilde, N. Miyakawa, P. Guptasarma, M. Iavarone, L. Ozyuzer, J.F. Zasadzinski, P. Roamno, D.G. Hinks, C. Kendziora, G.W. Crabtree, and K.E. Gray, *Phys. Rev. Lett.* **80**, 153 (1998).
- ¹⁷G.J. Strijkers, Y. Ji, F.Y. Yang, C.L. Chien, and J.M. Byers, *Phys. Rev. B* **63**, 104510 (2001).
- ¹⁸G.B. Arnold, *Phys. Rev. B* **23**, 1171 (1981).
- ¹⁹H. Schmidt, J.F. Zasadzinski, K.E. Gray, and D.G. Hinks, *Phys. Rev. B* **63**, 220504 (2001).
- ²⁰A. Kohen and G. Deutscher, *Phys. Rev. B* **64**, 060506(R) (2001).
- ²¹P. Samuely, Z. Holanová, P. Szabó, J. Kačmarčík, R.A. Ribeiro, S.L. Bud'ko, and P.C. Canfield, *Phys. Rev. B* **68**, 020505 (2003).
- ²²R.S. Gonnellia, A. Calzolaria, D. Dagheroa, G.A. Ummarinoa, V.A. Stepanovb, P. Finoc, G. Giunchid, S. Ceresarad, and G. Ripamontid, *J. Phys. Chem. Solids* **63**, 2319 (2002).
- ²³P. Martinez-Samper, J.G. Rodrigo, G. Rubio-Bollinger, H. Suderow, S. Vieira, S. Lee, and S. Tajima, *Physica C* **385**, 233 (2003).
- ²⁴N. Miyakawa, J.F. Zasadzinski, L. Ozyuzer, P. Guptasarma, D.G. Hinks, C. Kendziora, and K.E. Gray, *Phys. Rev. Lett.* **83**, 1018 (1999).
- ²⁵L. Ozyuzer, J.F. Zasadzinski, C. Kendziora, and K.E. Gray, *Phys. Rev. B* **61**, 3629 (2000).
- ²⁶P.A. Lee, *J. Appl. Phys.* **42**, 325 (1971).